Comparison of the device physics principles of planar and radial *p-n* junction nanorod solar cells

Brendan M. Kayes and Harry A. Atwater[a)]
Thomas J. Watson, Sr. Laboratories of Applied Physics, California Institute of Technology, MC 128-95, Pasadena, California 91125

Nathan S. Lewis[b)]
Arthur Amos Noyes Laboratories of Chemical Physics, California Institute of Technology, MC 127-72, Pasadena, California 91125

(Received 7 October 2004; accepted 15 March 2005; published online 23 May 2005)

A device physics model has been developed for radial *p-n* junction nanorod solar cells, in which densely packed nanorods, each having a *p-n* junction in the radial direction, are oriented with the rod axis parallel to the incident light direction. High-aspect-ratio (length/diameter) nanorods allow the use of a sufficient thickness of material to obtain good optical absorption while simultaneously providing short collection lengths for excited carriers in a direction normal to the light absorption. The short collection lengths facilitate the efficient collection of photogenerated carriers in materials with low minority-carrier diffusion lengths. The modeling indicates that the design of the radial *p-n* junction nanorod device should provide large improvements in efficiency relative to a conventional planar geometry *p-n* junction solar cell, provided that two conditions are satisfied: (1) In a planar solar cell made from the same absorber material, the diffusion length of minority carriers must be too low to allow for extraction of most of the light-generated carriers in the absorber thickness needed to obtain full light absorption. (2) The rate of carrier recombination in the depletion region must not be too large (for silicon this means that the carrier lifetimes in the depletion region must be longer than ~10 ns). If only condition (1) is satisfied, the modeling indicates that the radial cell design will offer only modest improvements in efficiency relative to a conventional planar cell design. Application to Si and GaAs nanorod solar cells is also discussed in detail. © *2005 American Institute of Physics*. [DOI: 10.1063/1.1901835]

I. INTRODUCTION

Inexpensive candidate materials for use in photovoltaic applications generally have either a high level of impurities or a high density of defects, resulting in low minority-carrier diffusion lengths.[1] The use of such low diffusion-length materials as the absorbing base in a conventional planar *p-n* junction solar-cell geometry results in devices having a carrier collection limited by minority-carrier diffusion in the base region (Fig. 1). Increasing the thickness of the base in such a cell will therefore produce more light absorption but will not result in an increase in device efficiency. In the absence of sophisticated light-trapping schemes, materials with low diffusion lengths and low absorption coefficients therefore cannot be readily incorporated into planar solar-cell structures with high energy-conversion efficiency.[2]

A semiconductor device consisting of arrays of radial *p-n* junction nanorods may provide a solution to this device design and optimization issue. A nanorod with a *p-n* junction in the radial direction would enable a decoupling of the requirements for light absorption and carrier extraction into orthogonal spatial directions. Each individual *p-n* junction nanorod in the cell could be long in the direction of incident light, allowing for optimal light absorption, but thin in another dimension, thereby allowing for effective carrier collection. Nanorod-fabrication techniques have progressed to the point where several materials can be incorporated into a single rod, and nanorods with *p-n* junctions in either the radial[3,4] or axial[5–8] directions have recently been reported. These advances open up the possibility of incorporating nanorods with *p-n* junctions in solar cells, if the significant difficulties associated with the fabrication of a full solar-cell device comprised of nanorods can be surmounted. Alternative approaches to achieving carrier collection in a direction perpendicular to light absorption have been investigated.[9–11]

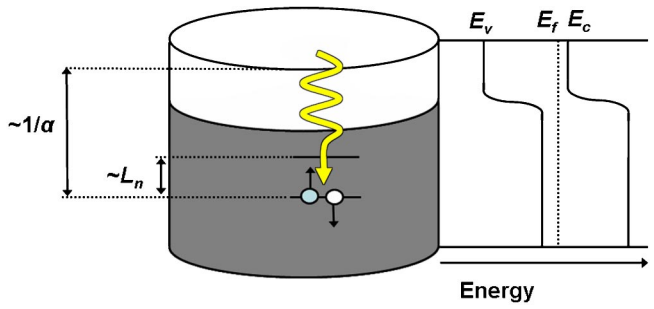

FIG. 1. (Color online) A conventional planar solar cell is a *p-n* junction device. Light penetration into the cell is characterized by the optical thickness of the material [$\sim 1/\alpha$, noting that the absorption coefficient α is wavelength dependent (see Sec. III B)], while the mean-free path of generated minority carriers is given by their diffusion length. In the case shown, light penetrates deep into the cell, but the electron-diffusion length is too short to allow for the collection of all light-generated carriers.

[a)]Electronic mail: haa@daedalus.caltech.edu
[b)]Electronic mail: nslewis@caltech.edu

The potential advantage of nanorod arrays lies in the ability in principle to prepare nanorods and nanorod arrays in a highly parallelized fashion, possibly allowing the design to be scaled up to large areas.

Although experimental methods to fabricate semiconductor nanostructures for photovoltaic applications are developing rapidly, much less attention has been given to the development of the device physics principles that govern the operation of nanostructured solar cells. Notably, a model for the charge transport in an excitonic, polymer/inorganic hybrid photovoltaic cell has recently been presented.[12] The work described herein addresses a different case, focusing on inorganic *p-n* junction solar cells in which the carriers are delocalized electrons and holes. Our model allows comparison between the device performance of the radial *p-n* junction nanorod cell geometry, as a function of the material properties and geometric device parameters of the cell, and the performance of a conventional planar cell geometry. The model involves solving the diffusion/drift equations for minority carriers, the current continuity equations, and Poisson's equation in the geometry of interest. The model has been applied to crystalline silicon and gallium arsenide, using a 100-mW/cm^2 Air Mass 1.5 spectrum, to obtain quantitative comparisons between the performance of the radial *p-n* junction nanorod geometry and the conventional planar *p-n* junction cell geometry. Cell efficiencies, open-circuit voltages, short-circuit current densities, and fill factors were calculated as a function of cell thickness (which is the same as the rod length in the nanorod case), nanorod radius, and electron-diffusion length at fixed emitter- and base-doping levels (sheath and core dopings in the nanorod case). Two regimes were treated—(1) the trap density was assumed constant through the material and thus the quasineutral-region and depletion-region lifetimes were coupled, and (2) the quasineutral-region trap density was assumed to be independent of the depletion-region trap density. The analysis considered purely inorganic homojunction and heterojunction devices with delocalized carriers and included the effects of free-carrier recombination, recombination at the junction, and surface recombination.

II. DEVICE PHYSICS MODELING

A. Device geometry and dimensions

The generalized band diagram and the geometries of the planar and radial *p-n* junction nanorod cell structures are depicted in Figs. 1–4. Both homojunctions and heterojunctions can be treated within the same general framework. The results for the planar case are well known[13] and will not be described in detail herein (see Appendix).

The model for the radial *p-n* junction nanorod solar cell was constructed by extending the analysis of the planar cell geometry[14] to a cylindrical geometry. The *p-n* junction in the nanorod was assumed to be abrupt, and the depletion approximation was assumed to be valid. The emitter layer (i.e., the exterior "shell" of the nanorod) was assumed to be *n* type, while the base (i.e., the interior "core" of the nanorod) was assumed to be *p* type. Light was assumed to be normally incident on the top face of the nanorod. Recombination was assumed to be purely due to the Shockley–Read–Hall recombination from a single-trap level at midgap;[15] other recombination processes, such as Auger recombination, were neglected. Surface-recombination effects were, however, included.

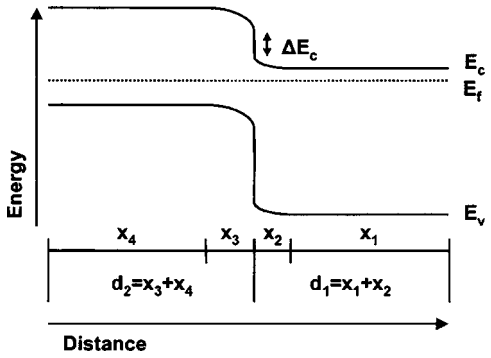

FIG. 2. Generalized band structure for a heterojunction nanorod structure. Shown are the conduction and valence band energies, E_c and E_v, as well as the Fermi energy E_f. ΔE_c is the discontinuity in the conduction band energy, which may be nonzero for a heterojunction. The example cells in this paper are homojunctions, and so $\Delta E_c = 0$. The x axis shows the schematic division of the cell into four regions: the quasineutral part of the *n*-type material (of width x_1), the depleted part of the *n*-type material (of width x_2), the depleted part of the *p*-type material (of width x_3), and the quasineutral part of the *p*-type material (of width x_4).

To simplify the analysis and to allow for analytic solutions, the carrier transport was taken to be purely radial. Although individual rods may have a high resistivity, the IR drop in a nanorod can still be very low because of the very small current that will pass through each rod. Given a resistivity $\sim 10^{-2}\ \Omega$ cm (appropriate for Si with doping $\sim 10^{18}$ cm^{-3}),[16] a rod length $\sim 100\ \mu$m, and a current density ~ 0.05 A cm^{-2}, the IR drop in a rod due to series resistance is $\sim 10^{-5}$ V. Hence, the exterior of the rod was assumed to be an equipotential surface relative to the core of the rod. The total photogenerated carrier flux was calculated by an integration that is equivalent to summing up the contributions at

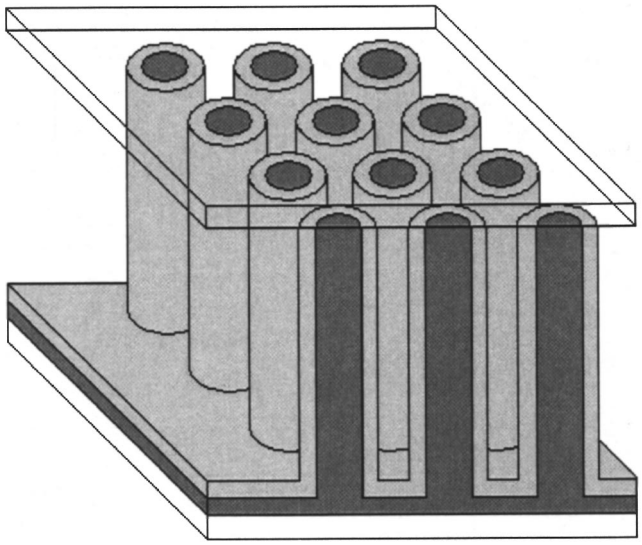

FIG. 3. Schematic cross-section of the radial *p-n* junction nanorod cell. Light is incident on the top surface. The light grey area is *n* type, the dark grey area *p* type.

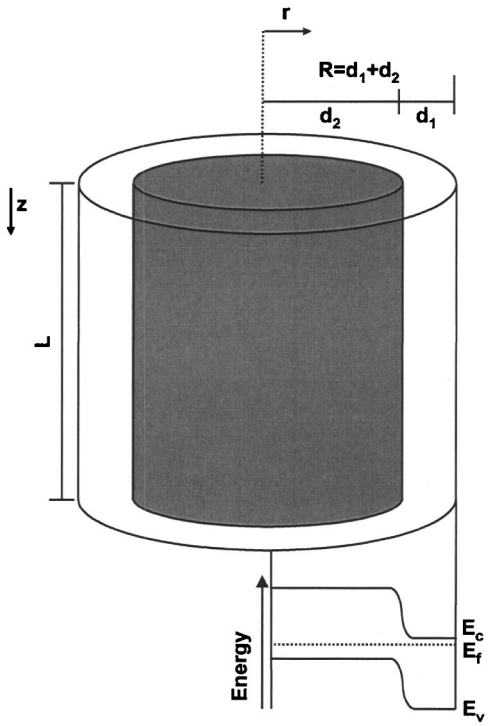

FIG. 4. Schematic of a single rod from the radial *p-n* junction nanorod cell and its corresponding energy band diagram. Light is incident on the top surface. The external shell is *n* type, the internal core is *p* type. E_c is the conduction band energy, E_v is the valence band energy, and E_f is the Fermi energy. The *n*-type material forms an annulus of width d_1; the *p*-type material has radius d_2. The total cell radius $R=d_1+d_2$, and its thickness is equal to the rod length L. Recombination at the top and bottom surfaces is neglected; i.e., it is assumed that minority-carrier diffusion in the vertical direction is negligible.

each value of z at a given bias, and the dark current was calculated for the entire junction area neglecting the ends. The bias was then varied, creating a current-density versus voltage (J-V) curve (not shown), from which the open-circuit voltage, short-circuit current density, fill factor, and efficiency could be calculated.

The approximation of one-dimensional carrier transport is valid when the variation in carrier concentration in the z direction occurs over a much longer length scale than that in the r direction. This is an appropriate assumption for a radial *p-n* junction nanorod in a material that is collection limited, that is, one with an optical thickness (see Sec. III B below) that is much greater than the diffusion length of minority carriers. In this case, the variation in carrier concentration in the axial direction is primarily due to light absorbtion and occurs over a large distance relative to the variation in carrier concentration in the radial direction, which occurs due to diffusion and drift resulting from the potential drop at the *p-n* junction interface.

A packing density of 100% was assumed. In practice, light will not be incident truly normal on the top surface of the rods, but rather at some angle. At small angles from normal incidence, light that is incident on the top of a rod will remain within the rod due to total internal reflection, while light that is not incident on the top of a rod is likely to pass through many rods while traversing the cell due to the high-aspect ratio of the rods. The precise details await further study.

B. Quasineutral part of the *p*-type region

The cell was divided schematically into four regions: the quasineutral part of the *n*-type region (of width x_1), the depletion region of the *n*-type material (of width x_2), the depletion region of the *p*-type material (of width x_3), and the quasineutral part of the *p*-type region (of width x_4) (Fig. 2). The minority-carrier movement in the quasineutral region of the *p*-type material was assumed to be governed by the transport equation,

$$\nabla^2 n' - \frac{n'}{L_n^{\,2}} = \frac{\partial^2 n'}{\partial r^2} + \frac{1}{r}\frac{\partial n'}{\partial r} - \frac{n'}{L_n^{\,2}} = -\frac{\alpha_2 \Gamma_0}{D_n} e^{-\alpha_2 x}, \tag{1}$$

where $n' = n - n_0$ is the excess minority-electron concentration with respect to the equilibrium value n_0, L_n is the diffusion length of minority electrons, α_2 is the absorption coefficient of the *p*-type material, Γ_0 is the incident photon flux, and D_n is the electron-diffusion coefficient. The boundary conditions were

$$n'(0) = \text{finite}, \tag{2}$$

$$n'(x_4) = n_0\left(e^{qV/kT} - 1\right), \tag{3}$$

where $q = 1.60219 \times 10^{-19}$ C is the magnitude of the electronic charge, V is the applied (forward) bias, $k = 1.3807 \times 10^{-23}$ m^2 kg s^{-2} K^{-1} is Boltzmann's constant, and the temperature T is assumed to be 300 K.

The current density in the *p*-type quasineutral region, J^p, is thus

$$J^p = \frac{2x_4 \int_0^L J^p(z)\,dz}{R^2}, \tag{4}$$

where

$$J^p(z) = -qD_n \left.\frac{\partial n'}{\partial r}\right|_{r=x_4}, \tag{5}$$

and R and L are the radius and length of the rod, respectively.

C. Quasineutral part of the *n*-type region

In the quasineutral region of the emitter, the transport equation is

$$\frac{\partial^2 p'}{\partial r^2} + \frac{1}{r}\frac{\partial p'}{\partial r} - \frac{p'}{L_p^{\,2}} = -\frac{\alpha_1 \Gamma_0}{D_p} e^{-\alpha_1 z}, \tag{6}$$

where $p' = p - p_0$ is the excess minority-hole concentration with respect to the equilibrium value p_0, L_p is the diffusion length of minority holes, α_1 is the absorption coefficient of the *n*-type material, and D_p is the hole-diffusion coefficient.

The boundary conditions were

$$p'(R - x_1) = p_0\left(e^{qV/kT} - 1\right), \tag{7}$$

$$S_p p'(R) = -D_p \left.\frac{\partial p'}{\partial r}\right|_{r=R}, \tag{8}$$

where S_p is the surface-recombination velocity of holes at the external surface of the rod. Hence, the current density in the n-type quasineutral region, J^n, is

$$J^n = \frac{2(R-x_1)\int_0^L J^n(z)dz}{R^2}, \tag{9}$$

where

$$J^n(z) = qD_p \left.\frac{\partial p'}{\partial r}\right|_{r=R-x_1}. \tag{10}$$

D. Depletion region

The light-generated current density in the depletion region, J_g^{dep}, was calculated by assuming that all absorbed incident light produced collected carriers. Hence, in the p-type part of the depletion region

$$J_g^{\text{dep},p}(V) = q\Gamma_0\left(1-e^{-\alpha_2 L}\right)\frac{{d_2}^2-{x_4}^2}{R^2}, \tag{11}$$

whereas in the n-type part of the depletion region

$$J_g^{\text{dep},n}(V) = q\Gamma_0\left(1-e^{-\alpha_1 L}\right)\frac{(d_2+x_2)^2-{d_2}^2}{R^2}. \tag{12}$$

The depletion region width was obtained by solving Poisson's equation in the depletion region, assuming that the electric field E was zero outside of the depletion region, that ϵE was continuous across the junction, where ϵ is the dielectric constant of the semiconductor, and that ionized donors and acceptors were the sole constituents of charge. The recombination current density in the depletion region was approximated by assuming that the potential in the depletion region was a linear function of r. The recombination current density for the entire depletion region was calculated by multiplying the maximum recombination rate by a small volume centered about this maximum recombination point, in analogy with the standard treatment of the planar case.[17]

III. RESULTS

Solving the above equations with the stated assumptions produced the following expression for the J-V behavior of the device:

$$J = (J_0^p + J_0^n)(e^{qV/kT}-1) - J_l^p - J_l^n - J_g^{\text{dep},p}(V) - J_g^{\text{dep},n}(V) + J_r^{\text{dep}}(V), \tag{13}$$

where

$$J_0^p = -2qn_0 L\frac{D_n}{{L_p}^2}\frac{\beta_5}{{\beta_1}^2}\frac{I_1(\beta_5)}{I_0(\beta_5)}, \tag{14}$$

$$J_0^n = -2qp_0 L\frac{D_p}{{L_p}^2}\frac{\beta_2}{{\beta_1}^2}\left(\frac{f_1K_1(\beta_2)-f_2I_1(\beta_2)}{f_1K_0(\beta_2)+f_2I_0(\beta_2)}\right), \tag{15}$$

$$J_l^p = -2q\Gamma_0\frac{{L_n}^2}{{L_p}^2}\frac{\beta_5}{{\beta_1}^2}\frac{I_1(\beta_5)}{I_0(\beta_5)}(1-e^{-\beta_6}), \tag{16}$$

$$J_l^n = -2q\Gamma_0\frac{\beta_2}{{\beta_1}^2}\times\left[\frac{K_1(\beta_2)(f_1-\beta_4 I_0(\beta_2))-I_1(\beta_2)(f_2+\beta_4 K_0(\beta_2))}{f_1K_0(\beta_2)+f_2I_0(\beta_2)}\right]\times(1-e^{-\beta_3}), \tag{17}$$

$$J_g^{\text{dep},p}(V) = -q\Gamma_0\frac{{d_2}^2-{x_4}^2}{R^2}(1-e^{-\beta_6}), \tag{18}$$

$$J_g^{\text{dep},n}(V) = -q\Gamma_0\frac{(d_2+x_2)^2-{d_2}^2}{R^2}(1-e^{-\beta_3}), \tag{19}$$

$$J_r^{\text{dep}}(V) = -qLU_{\max}\frac{{r_2}^2-{r_1}^2}{R^2}, \tag{20}$$

where $I_n(x)$ and $K_n(x)$, $n=0$ or 1, represent modified Bessel's functions of the first and second kinds, respectively.

The dimensionless parameters are defined as

$$\beta_1 = \frac{R}{L_p}, \tag{21}$$

$$\beta_2 = \frac{R-x_1}{L_p}, \tag{22}$$

$$\beta_3 = \alpha_1 L, \tag{23}$$

$$\beta_4 = \frac{L_p S_p}{D_p}, \tag{24}$$

$$\beta_5 = \frac{x_4}{L_n}, \tag{25}$$

$$\beta_6 = \alpha_2 L, \tag{26}$$

$$f_1 = f_1(\beta_1,\beta_4)$$

$$f_1 = I_1(\beta_1) + \beta_4 I_0(\beta_1), \tag{27}$$

$$f_2 = f_2(\beta_1,\beta_4)$$

$$f_2 = K_1(\beta_1) - \beta_4 K_0(\beta_1). \tag{28}$$

Additionally,

$$U_{\max} = \frac{n_{i,*}}{\sqrt{\tau_{n0}\tau_{p0}}}\sinh\left(\frac{qV}{2kT}\right), \tag{29}$$

$$r_1(V) = r(V) - \frac{(x_2(V)+x_3(V))}{2}\kappa, \tag{30}$$

$$r_2(V) = r(V) + \frac{(x_2(V)+x_3(V))}{2}\kappa, \tag{31}$$

$$r(V) = x_4 + \frac{\log\left(\frac{N_a}{n_{i,p}}\right)}{\log\left(\frac{N_a N_d}{n_{i,p} n_{i,n}}\right)}(x_2(V) + x_3(V)), \tag{32}$$

$$\kappa = \frac{\pi kT}{q(V_{\mathrm{bi}} - V)}, \tag{33}$$

$$V_{\mathrm{bi}} - V = \frac{qN_d}{2\varepsilon_n}(d_2 + x_2)^2 \log\left(\frac{d_2 + x_2}{d_2}\right) + \frac{qN_d}{4\varepsilon_n}\left[{d_2}^2 - (d_2 + x_2)^2\right] + \frac{qN_a}{2\varepsilon_p}{x_4}^2 \log\left(\frac{x_4}{d_2}\right) + \frac{qN_a}{4\varepsilon_p}({d_2}^2 - {x_4}^2), \tag{34}$$

where $N_a, n_{i,p}, \epsilon_p$, and τ_{n0} are the dopant (acceptor) density, intrinsic carrier concentration, dielectric constant, and lifetime in the depletion region, respectively, for the *p*-type material. $N_d, n_{i,n}, \epsilon_n$, and τ_{p0} are the analogous quantities for the *n*-type material. Also, $n_{i,*} = n_{i,p}$ or $n_{i,n}$, depending on whether the maximum recombination point lies in the *p*-type or *n*-type material. From Eq. (34), $x_2(V)$ and $x_3(V)$ can be found numerically, given the built-in voltage V_{bi}:

$$V_{\mathrm{bi}} = \frac{kT}{q}\log\left(\frac{N_a N_d}{n_{i,p} n_{i,n}}\right) + \frac{\Delta E_c}{q}, \tag{35}$$

where ΔE_c is the conduction-band offset (=0 for homojunctions).

A. Analytical assessment of nanorod solar-cell behavior

In the planar case, the model shows that the efficiency reaches a limiting value as the thickness increases.[18] In contrast, the efficiency of the radial *p-n* junction nanorod attains a maximum as a function of thickness—if the thickness is increased further, the efficiency is reduced. This behavior can be understood by realizing that the light-generated current density goes as

$$J_l \propto (1 - e^{-\alpha L}), \tag{36}$$

where α is the absorption coefficient of the material, and L is the cell thickness, while dark current density goes as

$$J_0 \propto L. \tag{37}$$

The competition between these two effects determines the optimum thickness of the radial *p-n* junction nanorod cell for attainment of the highest energy-conversion efficiency.

B. Numerical assessment of device behavior

To gain further insight into the behavior of the radial *p-n* junction cell, current-density versus voltage (*J-V*) curves were calculated for planar and radial *p-n* junction nanorod cells for silicon and gallium arsenide homojunctions (not shown). This set of simulations used the Air Mass 1.5 spectrum[19] and the optical-absorption coefficient as a function of energy for Si and GaAs.[20] The current density J was calculated at each value of the forward bias V and at each wavelength, and the results were numerically integrated over wavelength to obtain a value for the total current density as a function of bias.

Two regimes were treated—(1) the trap density was assumed constant through the material, and thus the minority-carrier lifetimes in the quasineutral region and in the depletion region were coupled, and (2) the trap density in the quasineutral region was assumed to be independent of the trap density in the depletion region. Depending on the specific fabrication process used to make a radial *p-n* junction nanorod solar cell, we anticipate that either set of assumptions could be realized in practice. The lifetimes in the depletion region are given by[21]

$$\tau_{n0} = \frac{1}{\sigma_n N_r v_{\mathrm{th}}}, \tag{38}$$

$$\tau_{p0} = \frac{1}{\sigma_p N_r v_{\mathrm{th}}}, \tag{39}$$

where σ_n and σ_p are the cross sections for electron and hole capture, respectively, N_r is the density of recombination centers, and v_{th} is the thermal velocity. To the first order, $\sigma_n = \sigma_p$, so that $\tau_{n0} = \tau_{p0}$. In case (1), the high doping levels we considered implies that[15]

$$\tau_n \approx \tau_{n0}, \tag{40}$$

$$\tau_p \approx \tau_{p0}, \tag{41}$$

so that $\tau_n = \tau_p = \tau_{n0} = \tau_{p0}$, where τ_n is the lifetime of minority electrons in the *p*-type quasineutral region, and τ_p is the lifetime of minority holes in the *n*-type quasineutral region. In turn, these lifetime values yield values for L_n and L_p through the relations[22]

$$L_n = \sqrt{\tau_n D_n}, \tag{42}$$

$$L_p = \sqrt{\tau_p D_p}, \tag{43}$$

where

$$D_{n,p} = \frac{kT}{q}\mu_{n,p}. \tag{44}$$

Hence in this situation only one parameter needs to be specified to determine the values of $\tau_n, \tau_p, \tau_{n0}, \tau_{p0}, L_n$, and L_p. In case (2), the assumption that $\tau_n = \tau_p$ and $\tau_{n0} = \tau_{p0}$ was retained, but τ_{n0} was held fixed (at 1 μs, or, equivalently, trap density N_r was held fixed at 10^{14} cm^{-3}), while τ_n was allowed to vary independently. Then the above relations were used to relate L_n and L_p to τ_n. This set of conditions simulated the situation in which the impurity profile was not constant throughout the sample. Case (2) led to quasineutral-region recombination being the dominant recombination mechanism.

The behavior of the cells was first investigated as a function of doping levels in the emitter and base, emitter thickness, and nanorod radius. Some general conditions for an optimal cell thus became apparent. At a given value of the minority-electron diffusion length, nanorod cells favored

high doping. The mobility was coupled to the doping through the relations given by the Ioffe Physico-Technical Institute,[23] the lifetime is related to the trap density in (38) and (39) above, and the mobility, lifetime, and diffusion length are related in (42)–(44). At a fixed trap density, increasing the doping will decrease the mobility and hence decrease the diffusion length. On the other hand, increasing the doping level will increase the built-in voltage, through Eq. (35). The detrimental effects of a low diffusion length are partially overcome by the nanorod geometry.

For a silicon cell, an n^+/p^+ structure was assumed, with the top layer and the external shell being n^+ in the planar and nanorod cells, respectively. The following parameters were used:[24]

$$N_d = 1 \times 10^{18}\ \mathrm{cm}^{-3},$$

$$N_a = 1 \times 10^{18}\ \mathrm{cm}^{-3},$$

$$\mu_p = 95\ \mathrm{cm}^2\ \mathrm{V}^{-1}\ \mathrm{s}^{-1},$$

$$\Rightarrow D_p = \frac{kT}{q}\mu_p = 2.46\ \mathrm{cm}^2\ \mathrm{s}^{-1},$$

$$\mu_n = 270\ \mathrm{cm}^2\ \mathrm{V}^{-1}\ \mathrm{s}^{-1},$$

$$\Rightarrow D_n = \frac{kT}{q}\mu_n = 6.98\ \mathrm{cm}^2\ \mathrm{s}^{-1},$$

$$d_1 = x_1 + x_2 \geqslant 1 \times 10^{-6}\ \mathrm{cm},$$

$$S_p = S_n = 1 \times 10^5\ \mathrm{cm\ s}^{-1},$$

$$\sigma_p = \sigma_n = 1 \times 10^{-15}\ \mathrm{cm}^2,$$

$$v_{\mathrm{th}} = 1 \times 10^7\ \mathrm{cm\ s}^{-1},$$

where the $\geqslant$ symbol indicates that d_1 was set equal to 1×10^{-6} cm, unless this was too small to allow the full voltage drop V_{bi} to occur across the *p-n* junction. In the latter case, d_1 was set equal to the minimum value required to achieve a voltage drop V_{bi}. The model assumes that the materials are not doped so heavily as to become degenerate;[25] also, the model does not account for Auger recombination.[26] Hence the doping was not set to an even higher value.

The simulations were also performed for a gallium arsenide homojunction cell. Gallium arsenide was chosen because it is an archetypal direct band-gap semiconductor, whose transport and optical properties are well known. GaAs is also a good light absorber compared with silicon (Fig. 5), in that the thickness of material required to absorb 90% of the power due to above-band-gap photons is 140 times greater in Si than in GaAs. This thickness, henceforth called the "optical thickness," is 125 μm for Si and is only 891 nm for GaAs. Thus, Si and GaAs represent two limiting cases with regard to absorption.

The following parameters were taken as a "baseline" scenario for the GaAs nanorod cell:[27]

$$N_d = 1 \times 10^{17}\ \mathrm{cm}^{-3},$$

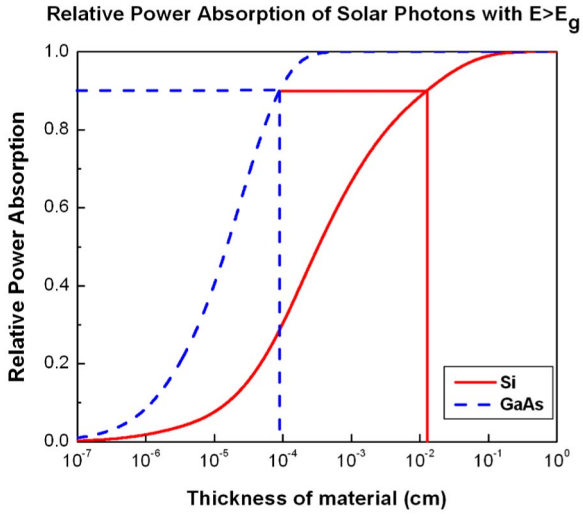

FIG. 5. (Color online) Relative light absorption—absorbed power for photons with energy greater than the band-gap energy vs thickness, for silicon and gallium arsenide.

$$N_a = 1 \times 10^{17}\ \mathrm{cm}^{-3},$$

$$\mu_p = 320\ \mathrm{cm}^2\ \mathrm{V}^{-1}\ \mathrm{s}^{-1},$$

$$\Rightarrow D_p = 8.27\ \mathrm{cm}^2\ \mathrm{s}^{-1}$$

$$\mu_n = 5000\ \mathrm{cm}^2\ \mathrm{V}^{-1}\ \mathrm{s}^{-1},$$

$$\Rightarrow D_n = 129\ \mathrm{cm}^2\ \mathrm{s}^{-1},$$

$$d_1 = x_1 + x_2 \geqslant 1 \times 10^{-6}\ \mathrm{cm},$$

$$S_p = S_n = 1 \times 10^5\ \mathrm{cm\ s}^{-1},$$

$$\sigma_p = \sigma_n = 1 \times 10^{-15}\ \mathrm{cm}^2,$$

$$v_{\mathrm{th}} = 1 \times 10^7\ \mathrm{cm\ s}^{-1}.$$

As for silicon, the maximum doping level was limited by the need to have a nondegenerate material,[28] the recombination of which is not dominated by Auger processes.[29]

The results for Si are shown in Figs. 6–8, while those for GaAs are shown in Figs. 9–11.

IV. DISCUSSION

The trends in cell performance computed for Si and GaAs contain important similarities as well as important differences, with the differences between the two systems appearing due to the different length scales involved. The simulations therefore suggest some general features about the operation of the radial *p-n* junction nanorod solar cell relative to the planar-junction cell geometry, as described herein.

A. Short-circuit current density, silicon

As shown in Fig. 6, the short-circuit current density J_{sc} in the silicon nanorod cell is essentially independent of the trap density (recall, from Eqs. (38)–(43) above, that L_n

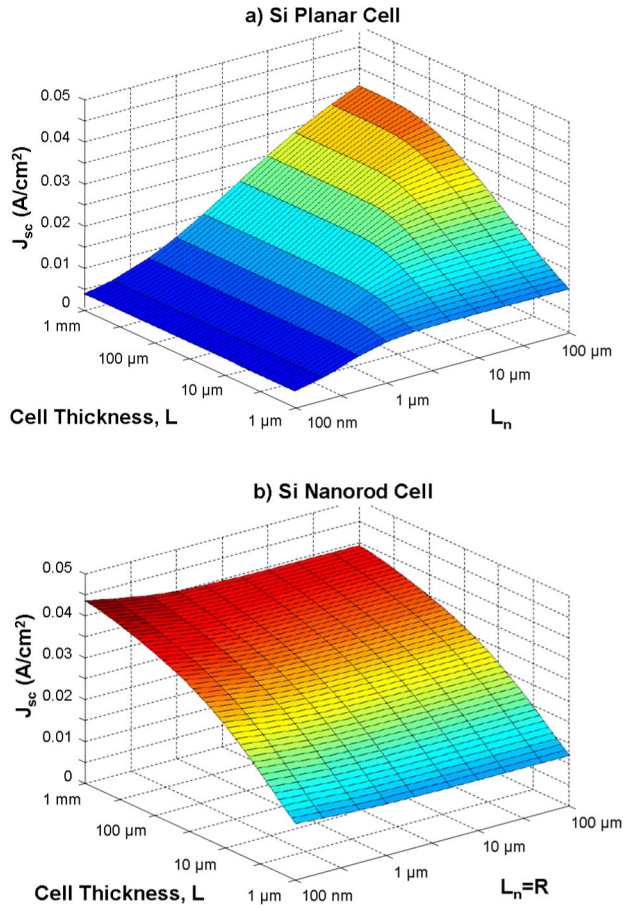

FIG. 6. (Color online) Short-circuit current density J_{sc} vs cell thickness L and minority-electron diffusion length L_n for (a) a conventional planar p-n junction silicon cell and (b) a radial p-n junction nanorod silicon cell. In both cases the short-circuit current density is unaffected by decreasing the trap density in the depletion region. In the radial p-n junction nanorod case, the cell radius R is set equal to L_n, a condition that was found to be near optimal.

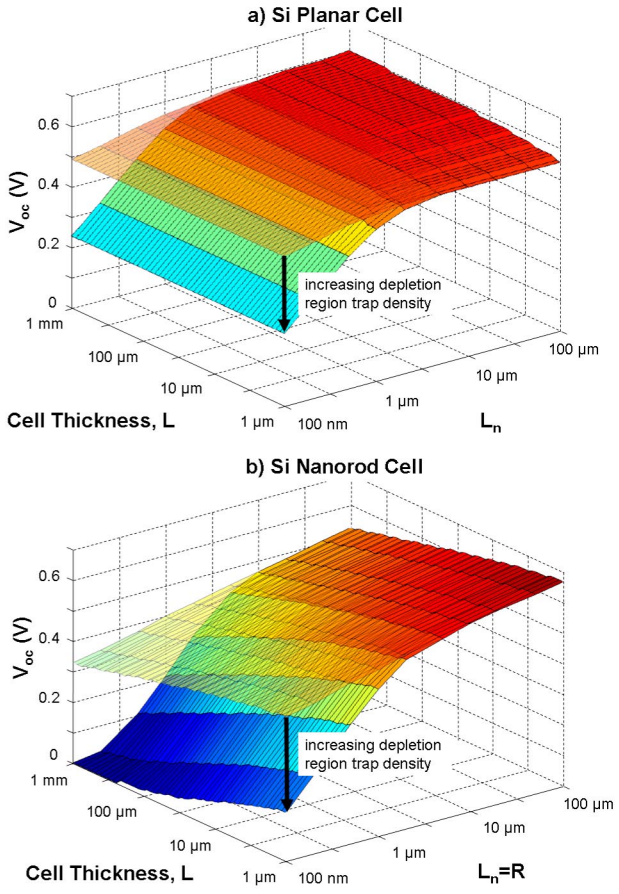

FIG. 7. (Color online) Open-circuit voltage V_{oc} vs cell thickness L and minority-electron diffusion length L_n for (a) a conventional planar p-n junction silicon cell and (b) a radial p-n junction nanorod silicon cell. In both cases the top surface shown in the plot has a depletion-region trap density fixed at 10^{14} cm^{-3}, so that $\tau_{n0}, \tau_{p0} = 1$ μs, while the bottom surface has a depletion-region trap density equal to the trap density in the quasineutral region, at each value of L_n. In the radial p-n junction nanorod case, the cell radius R is set equal to L_n, a condition that was found to be near optimal.

$\propto 1/\sqrt{N_r}$), in stark contrast to the planar cell. For a 100-μm-thick silicon solar cell, J_{sc} in the radial p-n junction nanorod geometry was $\approx$38 mA/cm^2 for thin (100-nm radius) rods, decreasing slightly to $\approx$35 mA/cm^2 as the rod radius increased above 1 μm, whereas in the planar geometry J_{sc} dropped from 34 to 4 mA/cm^2 as N_r increased from 7×10^{12} to 7×10^{18} cm^{-3} (so that L_n dropped from 100 μm to 100 nm in the quasineutral region of the p-type material). Note that a silicon cell of thickness $L=100$ μm is not optically thick, in that it absorbs less than 90% of the power from incident photons with energy above the band gap (see Sec. III B above). J_{sc} approached $\sim$43 mA/cm^2 in both geometries as L_n approached 1 mm, in the limit of large L ($>$1 mm). The radial p-n junction design overcomes the problems of carrier collection that are present in the conventional planar geometry. These results, for both planar and radial p-n junction nanorod cells, were unaffected by decreasing the trap density in the depletion region.

B. Open-circuit voltage, silicon

The degree to which the open-circuit voltage varied with the trap density depended most strongly on the trap density in the depletion region, for both the radial p-n junction case and for the planar case (Fig. 7). A low trap density in the depletion region produced a relatively high open-circuit voltage even if the quasineutral-region trap density was relatively high.

In the planar case, the open-circuit voltage is independent of cell thickness and decreases as the quasineutral-region electron-diffusion length decreases—slowly if the lifetime in the depletion region is held fixed at a relatively high value, and more rapidly if the trap densities are the same in both regions. In the radial p-n junction case, the open-circuit voltage decreases as the cell thickness increases because the junction area increases. Also, the open-circuit voltage decreases as the electron-diffusion length decreases in the quasineutral region—slowly if the lifetime in the depletion region is held fixed at a relatively high value, and rapidly if the trap densities are the same in both regions. For a 100-μm-thick silicon solar cell, the open-circuit voltage in the radial p-n junction nanorod geometry dropped from 0.58 to 0.01 V as N_r increased from 7×10^{12} to 7×10^{18} cm^{-3}, but only dropped from 0.58 to 0.38 V if N_r in the depletion region was held fixed at 10^{14} cm^{-3}. In the planar geometry

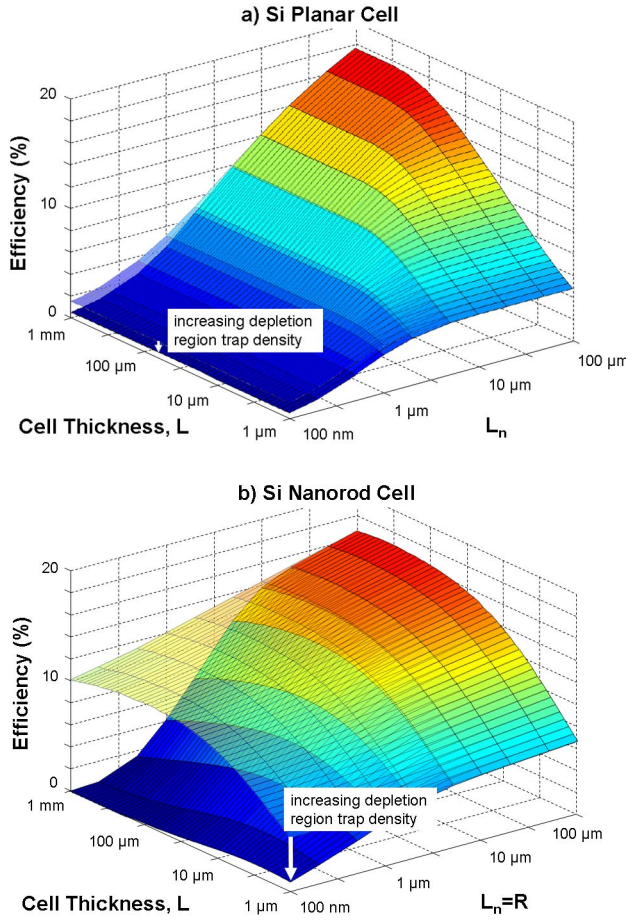

FIG. 8. (Color online) Efficiency vs cell thickness L and minority-electron diffusion length L_n for (a) a conventional planar p-n junction silicon cell and (b) a radial p-n junction nanorod silicon cell. In both cases the top surface shown in the plot has a depletion-region trap density fixed at 10^{14} cm^{-3}, so that $\tau_{n0}, \tau_{p0} = 1$ μs, while the bottom surface has a depletion-region trap density equal to the trap density in the quasineutral region, at each value of L_n. In the radial p-n junction nanorod case, the cell radius R is set equal to L_n, a condition that was found to be near optimal.

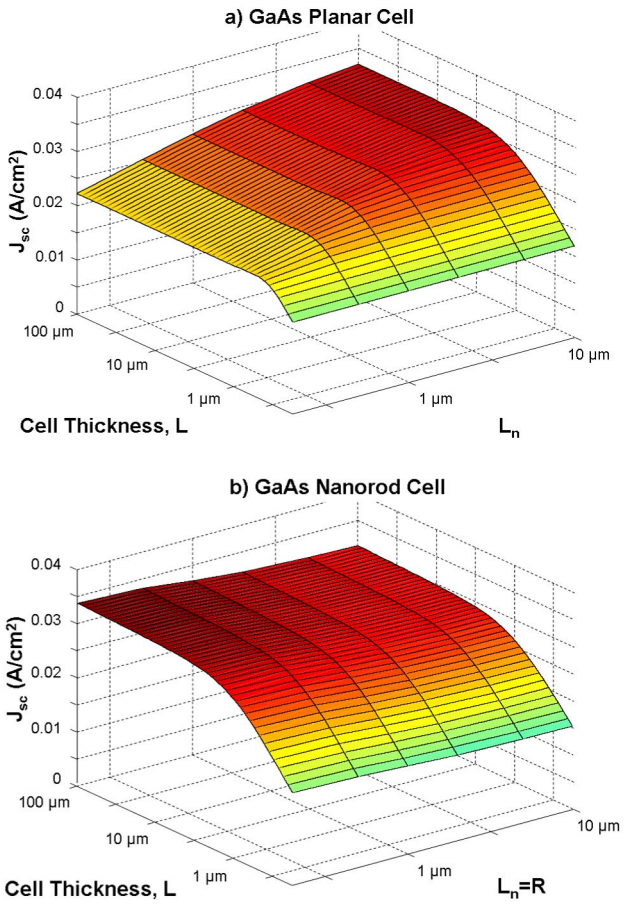

FIG. 9. (Color online) Short-circuit current density J_{sc} vs cell thickness L and minority-electron diffusion length L_n for (a) a conventional planar p-n junction gallium arsenide cell and (b) a radial p-n junction nanorod gallium arsenide cell. In both cases the short-circuit current density is unaffected by decreasing the trap density in the depletion region. In the radial p-n junction nanorod case, the cell radius R is set equal to L_n, a condition that was found to be near optimal.

the open-circuit voltage dropped from 0.59 to 0.24 V over the same range, or from 0.59 to 0.49 V if N_r in the depletion region was held fixed.

C. Cell efficiency, silicon

Taken together, the factors discussed above imply that the efficiency of a radial p-n junction nanorod solar cell can remain high despite a high quasineutral-region trap density, provided that the depletion-region trap density remains relatively low (Fig. 8). In the planar geometry, a high quasineutral-region trap density leads to a very low short-circuit current density, regardless of the trap density in the depletion region. This behavior inevitably results in a low efficiency for such systems [Fig. 8(a)]. In contrast, for the radial p-n junction, the short-circuit current density can attain high values even for very large trap densities in both the quasineutral regions and the depletion region. The open-circuit voltage, and thus the overall efficiency, can remain high, provided that the trap density in the depletion region is relatively low.

For a silicon solar cell with $L_n = 100$ nm (so that $N_r \approx 7 \times 10^{18}$ cm^{-3}) in the quasineutral regions and $N_r = 10^{14}$ cm^{-3} in the depletion region, the maximal efficiency of the radial p-n junction nanorod geometry was 11%, compared with 1.5% in the planar geometry. This maximal efficiency occurred for a radial p-n junction nanorod cell between 20 and 500 μm thick, whereas the efficiency saturated for a planar cell thicker than 450 nm. If N_r was set to 7×10^{18} cm^{-3} throughout the cell, the maximal efficiency of the radial p-n junction nanorod geometry was 1%, compared with 0.5% in the planar geometry. In this case, the maximal efficiency occurred for a radial p-n junction nanorod cell between 1 and 30 μm thick, whereas the efficiency saturated for a planar cell thicker than 1 μm.

For a silicon solar cell with $L_n = 1$ μm (so that $N_r \approx 7 \times 10^{16}$ cm^{-3}) in the quasineutral regions and $N_r = 10^{14}$ cm^{-3} in the depletion region, the maximal efficiency of the radial p-n junction nanorod geometry was 13%, compared with 5% in the planar geometry. This maximal efficiency occurred for a radial p-n junction nanorod cell between 100 and 240 μm thick, whereas the efficiency saturated for a planar cell thicker than 5 μm. If N_r was set to 7×10^{16} cm^{-3} throughout the cell, the maximal efficiency of the radial p-n junction

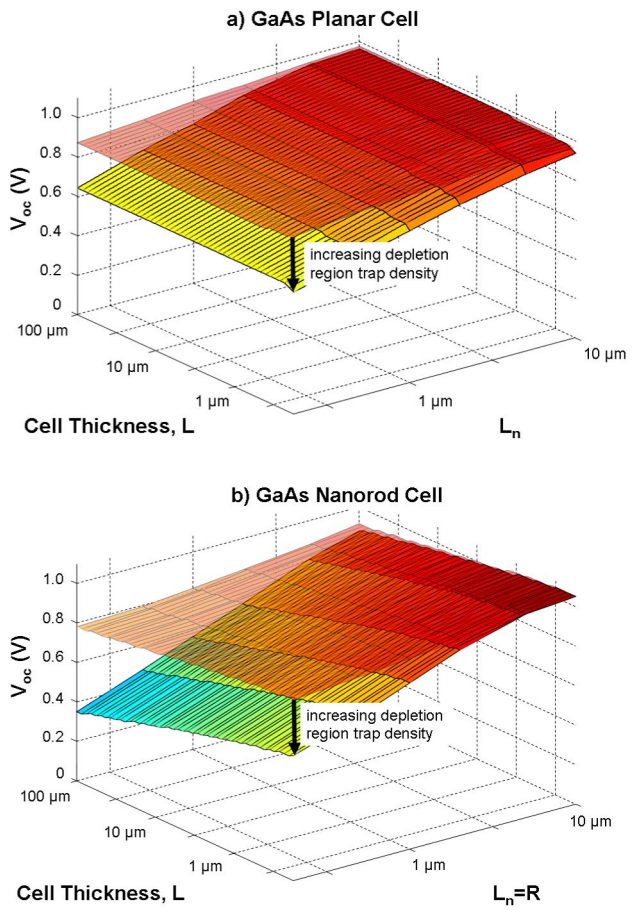

FIG. 10. (Color online) Open-circuit voltage V_{oc} vs cell thickness L and minority-electron diffusion length L_n for (a) a conventional planar *p-n* junction gallium arsenide cell and (b) a radial *p-n* junction nanorod gallium arsenide cell. In both cases the top surface shown in the plot has a depletion-region trap density fixed at 10^{14} cm^{-3}, so that $\tau_{n0}, \tau_{p0}=1$ μs, while the bottom surface has a depletion-region trap density equal to the trap density in the quasineutral region, at each value of L_n. In the radial *p-n* junction nanorod case, the cell radius R is set equal to L_n, a condition that was found to be near optimal.

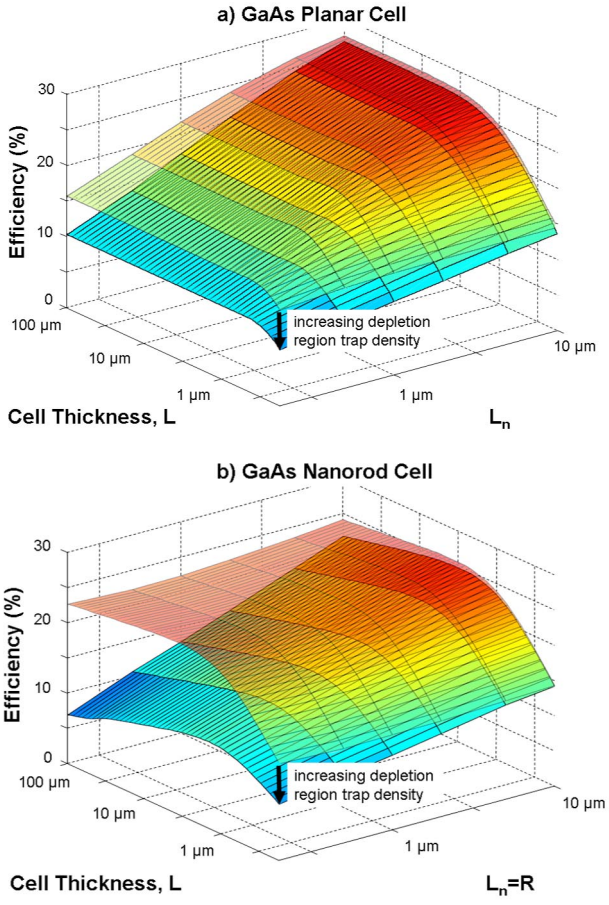

FIG. 11. (Color online) Efficiency vs cell thickness L and minority-electron diffusion length L_n for (a) a conventional planar *p-n* junction gallium arsenide cell and (b) a radial *p-n* junction nanorod gallium arsenide cell. In both cases the top surface shown in the plot has a depletion region trap density fixed at 10^{14} cm^{-3}, so that $\tau_{n0}, \tau_{p0}=1$ μs, while the bottom surface has a depletion-region trap density equal to the trap density in the quasineutral region, at each value of L_n. In the radial *p-n* junction nanorod case, the cell radius R is set equal to L_n, a condition that was found to be near optimal.

nanorod geometry was 7%, compared with 4% in the planar geometry. In this case, the maximal efficiency occurred for a radial *p-n* junction nanorod cell between 5 and 100 μm thick, whereas the efficiency saturated for a planar cell thicker than 5 μm.

D. Fill factor, silicon

The fill factor was nearly constant at ~0.8 as a function of L and L_n for both planar and radial geometries in the case that $\tau_{n0}=\tau_{p0}=1$ μs (so that $N_r \approx 10^{14}$ cm^{-3} in the depletion region), reaching a maximum of ~0.84 within the range of L, R, and L_n considered (graphs not shown). In the case that $\tau_{n0}=\tau_{p0}=\tau_n=\tau_p$, the fill factor began to drop for $L_n \leqslant 5$ μm (i.e., for $N_r > \sim 3\times 10^{15}$ cm^{-3}), steeply for the radial *p-n* junction nanorod and more gradually for the planar cell.

E. Gallium arsenide

The results for short-circuit current density, open-circuit voltage, and overall cell efficiency for GaAs are presented in Figs. 9–11, respectively. Clearly, the performance difference between the planar and nanorod structures for GaAs is not nearly as dramatic as that for Si. This is due simply to the change in the relative length scales involved with the direct band-gap material. As noted above, the optical thickness of GaAs is 891 nm. Therefore, severely collection-limited GaAs planar cells must have diffusion lengths much less than 891 nm, i.e., on the order of tens of nanometers or less. Recall also that the dopant density determines the depletion region width, with higher doping leading to thinner depletion regions. Nondegenerate doping implies that depletion regions in GaAs are on the order of hundreds of nanometers (191 nm for the planar case in our simulation. In the radial geometry the depletion region width depends upon the value of x_4, with 191 nm setting a lower bound). Making a radial *p-n* junction with a radius equal to the minority-electron diffusion length, that is, less than ~100 nm for severely collection-limited GaAs, thus results in fully depleted *p-n* junctions. This is a problem for two reasons. First, a fully depleted cell cannot attain its full built-in voltage as given in Eq. (35), and the built-in voltage drops rapidly as the cell radius decreases further.[30] Second, a fully depleted cell by

definition has no quasineutral region; therefore, the concept of keeping the trap density in the depletion region low while the trap density in the quasineutral regions increases is meaningless. If the cell is fully depleted, then the lifetime in the depletion region, which needs to be high, is in fact the lifetime in the whole rod, and this defeats the whole concept of using lower lifetime material in the nanorod geometry.

Note, however, that, as for the silicon case, the short-circuit current density in the radial *p-n* junction nanorod cell does not decrease with increasing trap density. This is not true in the planar geometry. Thus, it may be possible that degenerately doped GaAs radial *p-n* junction nanorods could exhibit some of the performance advantages seen in nondegenerately doped Si. This, however, is left to the subject of a future study that deals explicitly with the transport and statistics of degenerately doped systems.

F. General trends

Further insight into the differences between the two cell geometries was obtained by evaluating the efficiency, V_{oc}, and J_{sc}, versus L and R for a radial *p-n* junction nanorod cell (figures not shown). J_{sc} increased with increasing rod length, plateauing when the length of the rod became much greater than the optical thickness of the material. Also, J_{sc} was essentially independent of rod radius, provided that the radius was less than L_n. The value of J_{sc} decreased steeply for $R > L_n$. J_{sc} was essentially independent of trap density in the depletion region.

The open circuit voltage V_{oc} decreased with increasing rod length, and increased with increasing rod radius. The extent to which V_{oc} decreased with increasing rod length depended strongly on the trap density in the depletion region: as the trap density became high ($>\sim 3\times10^{15}$ cm^{-3} for Si, $>\sim 5\times10^{16}$ cm^{-3} for GaAs) in the depletion region, the V_{oc} declined rapidly. The trap density in the quasineutral regions, on the other hand, had relatively less effect on V_{oc}.

The optimal rod dimensions are obtained when the rod has a radius approximately equal to L_n and a length that is determined by the specific trade-off between the increase in J_{sc} and the decrease in V_{oc} with length. If the trap density in the depletion region is relatively low (i.e., $<\sim 3\times10^{15}$ cm^{-3} for Si, $<\sim 5\times10^{16}$ cm^{-3} for GaAs), the maximum efficiency occurs for rods having a length approximately equal to the optical thickness. For higher trap densities in the depletion region, smaller rod lengths are optimal.

Radial *p-n* junction nanorod cells tend to favor high doping levels to produce high cell efficiencies. High doping will lead to a decreased charge-carrier mobility and a decreased depletion region width, but in turn high doping advantageously increases the built-in voltage. Because carriers can travel approximately one diffusion length through a quasineutral region before recombining, making the rod radius approximately equal to the minority-electron diffusion length allows carriers to traverse the cell even if the diffusion length is low, provided that the trap density is relatively low in the depletion region.

An optimally designed radial *p-n* junction nanorod cell should be doped as highly as possible in both *n*- and *p*-type regions, have a narrow emitter width, have a radius approximately equal to the diffusion length of electrons in the *p*-type core (in qualitative agreement with Kannan *et al.*[12]), and have a length approximately equal to the optical thickness of the material. It is crucial that the trap density near the *p-n* junction is relatively low. Therefore one would prefer to use a doping mechanism that will getter impurities away from the junction.

V. CONCLUSIONS

In summary, the radial *p-n* junction nanorod geometry has the potential to produce significant improvements in efficiencies of cells made from materials that have diffusion lengths that are low relative to their optical thickness (at least two orders of magnitude less than the optical thickness) and low depletion region recombination (depletion region lifetimes $>\sim 10$ ns for silicon). Optimal cells have a radius approximately equal to the minority-electron diffusion length in the *p*-type core, and their doping levels must be high enough that a rod of such radius is not fully depleted. In silicon with very low diffusion lengths ($L_n = 100$ nm), extremely large efficiency gains (from 1.5% to 11%) are possible by exploiting the radial *p-n* junction nanorod geometry, provided that the trap density in the depletion region is held fixed at a relatively low level ($<\sim 3\times10^{15}$ cm^{-3}). This increase is explained by the greatly enhanced carrier collection that is possible in the radial *p-n* junction nanorod cell and is a verification of the principle of exploiting geometry to extract carriers from optically thick, low-diffusion-length solar cell materials. We anticipate that the results presented here can motivate the design of new types of nanorod solar cells that may enable efficient carrier collection in inorganic solar absorber materials with low minority-carrier diffusion lengths.

ACKNOWLEDGMENT

This work was supported by the National Renewable Energy Laboratory.

APPENDIX: PLANAR CELL EQUATIONS

The equations above (see Section II) can be solved in the planar geometry to give the current density in a planar cell as the sum of the current density in the quasineutral regions and the current density in the depletion region,

$$J = (J_0^p + J_0^n)(e^{qV/kT} - 1) - J_l^p - J_l^n - J_g^{\mathrm{dep}}(V) + J_r^{\mathrm{dep}}(V), \qquad \text{(A1)}$$

where

$$J_0^p = -\left(\frac{qD_n}{L_n}\right) n_0 \left[\frac{(S_n L_n/D_n)\cosh(x_4/L_n) + \sinh(x_4/L_n)}{(S_n L_n/D_n)\sinh(x_4/L_n) + \cosh(x_4/L_n)}\right], \qquad \text{(A2)}$$

$$J_0^n = -\left(\frac{qD_p}{L_p}\right) p_0 \left[\frac{(S_p L_p/D_p)\cosh(x_1/L_p) + \sinh(x_1/L_p)}{(S_p L_p/D_p)\sinh(x_1/L_p) + \cosh(x_1/L_p)}\right], \qquad \text{(A3)}$$

$$J_l^p = -\frac{q\Gamma_0 e^{-a_1 d_1 - \alpha_2 x_3}}{1-\alpha_2{}^{-2}L_n{}^{-2}}\left\{1-\frac{1}{\alpha_2 L_n}\left[\frac{(S_n L_n/D_n)(\cosh(x_4/L_n)-e^{-a_2 x_4})+\sinh(x_4/L_n)+\alpha_2 L_n e^{-\alpha_2 x_4}}{(S_n L_n/D_n)\sinh(x_4/L_n)+\cosh(x_4/L_n)}\right]\right\}, \tag{A4}$$

$$J_l^n = -\frac{q\Gamma_0}{1-\alpha_1{}^{-2}L_p{}^{-2}}\left\{\frac{(S_p/\alpha_1 D_p)+1-[(S_p/\alpha_1 D_p)\cosh(x_1/L_p)+(1/\alpha_1 L_p)\sinh(x_1/L_p)]e^{-\alpha_1 x_1}}{(S_p L_p/D_p)\sinh(x_1/L_p)+\cosh(x_1/L_p)}-e^{-\alpha_1 x_1}\right\}, \tag{A5}$$

$$J_g^{\mathrm{dep}}(V) = -q\Gamma_0 e^{-\alpha_1 x_1}\left(1-e^{-\alpha_1 x_2(V)-\alpha_2 x_3(V)}\right), \tag{A6}$$

where

$$x_3(V) = \left[\frac{2N_d\varepsilon_n\varepsilon_p(V_{\mathrm{bi}}-V)}{qN_a(N_d\varepsilon_n+N_a\varepsilon_p)}\right]^{1/2}, \tag{A7}$$

$$x_2(V) = \left[\frac{2N_a\varepsilon_n\varepsilon_p(V_{\mathrm{bi}}-V)}{qN_d(N_d\varepsilon_n+N_a\varepsilon_p)}\right]^{1/2}, \tag{A8}$$

$$V_{\mathrm{bi}} = \frac{kT}{q}\log\left(\frac{N_a N_d}{n_{i,p}n_{i,n}}\right)+\frac{\Delta E_c}{q}, \tag{A9}$$

and S_n is the surface recombination velocity of minority electrons at the bottom surface of the cell. The other symbols are defined above. The recombination current density in the depletion region is given, for a planar homojunction, by

$$J_r^{\mathrm{dep}}(V) = -\frac{qn_i(x_2+x_3)}{\sqrt{\tau_{n0}\tau_{p0}}}\left[\frac{2\sinh(qV/(2kT))}{q(V_{\mathrm{bi}}-V)/(kT)}\right]\frac{\pi}{2}. \tag{A10}$$

[1] V. Schlosser, IEEE Trans. Electron Devices **31**, 610 (1984).
[2] M. Imaizumi, T. Ito, M. Yamaguchi, and K. Kaneko, J. Appl. Phys. **81**, 7635 (1997).
[3] J. Goldberger, R. R. He, Y. F. Zhang, S. W. Lee, H. Q. Yan, H. J. Choi, and P. D. Yang, Nature (London) **422**, 599 (2003).
[4] L. J. Lauhon, M. S. Gudiksen, D. Wang, and C. M. Lieber, Nature (London) **420**, 57 (2002).
[5] K. Haraguchi, T. Katsuyama, K. Hiruma, and K. Ogawa, Appl. Phys. Lett. **60**, 745 (1992).
[6] Y. Y. Wu, R. Fan, and P. D. Yang, Nano Lett. **2**, 83 (2002).
[7] M. T. Bjork *et al.*, Nano Lett. **2**, 87 (2002).
[8] M. S. Gudiksen, L. J. Lauhon, J. Wang, D. C. Smith, and C. M. Lieber, Nature (London) **415**, 617 (2002).
[9] M. A. Green and S. R. Wenham, Appl. Phys. Lett. **65**, 2907 (1994).
[10] K. J. Weber, A. W. Blakers, M. J. Stocks, J. H. Babaei, V. A. Everett, A. J. Neuendorf, and P. J. Verlinden, IEEE Electron Device Lett. **25**, 37 (2004).
[11] K. Taretto and U. Rau, Prog. Photovoltaics **12**, 573 (2004).
[12] B. Kannan, K. Castelino, and A. Majumdar, Nano Lett. **3**, 1729 (2003).
[13] See Appendix. Also see, for example, A. Fahrenbruch and R. Bube, *Fundamentals of Solar Cells: Photovoltaic Solar Energy Conversion* (Academic, Stanford, 1983); or S. J. Fonash, *Solar Cell Device Physics* (Academic, New York, 1981).
[14] A. Fahrenbruch and R. Bube, *Fundamentals of Solar Cells: Photovoltaic Solar Energy Conversion* (Academic, Stanford, 1983).
[15] W. Shockley and W. T. Read, Phys. Rev. **87**, 835 (1952).
[16] http://www.ioffe.rssi.ru/SVA/NSM/Semicond/Si/Figs/135.gif
[17] C. T. Sah, R. N. Noyce, and W. Shockley, Proc. IRE **45**, 1228 (1957).
[18] In practice, this is not strictly true; it reflects the fact that the model only considers minority carrier transport. In particular, majority-carrier recombination is neglected. In reality, majority carriers will recombine also. However, the length scale associated with majority-carrier recombination will be much longer than for minority carriers, and thus, to a good approximation, majority-carrier recombination may be neglected.
[19] Air Mass 1.5 Global Spectrum, UNSW Key Center for Photovoltaic Engineering, http://www.pv.unsw.edu.au/am1.5.html. This website is now defunct - for the AM 1.5 spectrum please see http://rredc.nrel.gov/solar/
[20] n,k data from *Handbook of Optical Constants of Solids*, edited by E. D. Palik (Academic, Orlando, 1998).
[21] R. F. Pierret, *Advanced Semiconductor Fundamentals*, 2nd ed. (Prentice-Hall, Englewood Cliffs, NJ, 2003), pp. 148, 149, and 154.
[22] R. F. Pierret, *Semiconductor Fundamentals*, 2nd ed. (Addison-Wesley, Reading, MA, 1988), p. 99.
[23] http://www.ioffe.rssi.ru/SVA/NSM/Semicond/Si/electric.html; http://www.ioffe.rssi.ru/SVA/NSM/Semicond/GaAs/electric.html
[24] Use was made of information from the website of the Ioffe Physico-Technical Institute, "Electronic archive: New Semiconductor Materials. Characteristics and Properties," http://www.ioffe.rssi.ru/SVA/NSM/Semicond/Si/electric.html
[25] A semiconductor is termed "degenerate" if $E_c - E_f < 3$ kT, or if $E_f - E_v < 3$ kT. This occurs in silicon for dopings above $\sim 1\times 10^{18}$ cm^{-3}. See R. F. Pierret, in Ref. 21, pp. 115 and 127.
[26] The onset of Auger recombination can be estimated by the change in slope in a plot of lifetime vs dopant density. For silicon this occurs at dopant densities of $\sim 5\times 10^{18}$ cm^{-3}. See http://www.ioffe.rssi.ru/SVA/NSM/Semicond/Si/Figs/1323.gif
[27] Again, use was made of information from the website of the Ioffe Physico-Technical Institute, http://www.ioffe.rssi.ru/SVA/NSM/Semicond/GaAs/electric.html
[28] GaAs becomes degenerate for dopings above $\sim 1\times 10^{17}$ cm^{-3}. See Ref. 25 above.
[29] Auger recombination begins to dominate in GaAs at doping levels above $\sim 1\times 10^{19}$ cm^{-3}. See R. K. Ahrenkiel, R. Ellingson, W. Metzger, D. I. Lubyshev, and W. K. Liu, Appl. Phys. Lett. **78**, 1879 (2001).
[30] This is simply because there are not enough dopant ions to create the voltage drop required.